Male-specific colon motility dysfunction in the TashT mouse line

Journal:	*Neurogastroenterology and Motility*
Manuscript ID	NMO-00012-2016.R2
Manuscript Type:	Original Article
Date Submitted by the Author:	n/a
Complete List of Authors:	Touré, Aboubacrine; Universite du Quebec a Montreal, Sciences biologiques Charrier, Baptiste; Universite du Quebec a Montreal, Sciences biologiques Pilon, Nicolas; Universite du Quebec a Montreal, Sciences biologiques
Key Words:	Chronic constipation, Enteric nervous system, Hirschsprung's disease, Myenteric plexus

Male-specific colon motility dysfunction in the *TashT* mouse line

Aboubacrine Mahamane Touré, Baptiste Charrier and Nicolas Pilon

Molecular Genetics of Development Laboratory, Department of Biological Sciences and BioMed Research Center, Faculty of Sciences, University of Quebec at Montreal (UQAM), Montreal, Canada.

Correspondence to: Nicolas Pilon, Department of Biological Sciences and BioMed Research Center, Faculty of Sciences, University of Quebec at Montreal (UQAM), 141 President-Kennedy Ave, Montreal, PQ, Canada, H2X 3Y7; Tel.: 514-987-3000 x3342; Fax: 514-987-4647; Email: pilon.nicolas@uqam.ca

KEY MESSAGES

- In the *TashT* mouse model of Hirschsprung disease, an important subset of homozygous animals do not develop aganglionic megacolon despite having distal colon aganglionosis and/or hypoganglionosis.
- Both distal colon aganglionosis and hypoganglionosis are more severe in *TashT*$^{Tg/Tg}$ males.
- *TashT*$^{Tg/Tg}$ males, but not females, display altered distal colonic motility independently of aganglionosis.
- An increase of nitrergic neurons that is restricted to the most distal ganglionated regions is also observed in *TashT*$^{Tg/Tg}$ males but not in females.

ABSTRACT

***Background*:** In Hirschsprung disease (HSCR), the absence of myenteric neural ganglia in the distal bowel prevents motility and thereby causes functional intestinal obstruction. Although surgical resection of the aganglionic segment allows HSCR children to survive this condition, a number of patients still suffer from impaired motility despite having myenteric ganglia in their postoperative distal bowel. Such phenomenon is also observed in patients suffering from other enteric neuropathies and, in both cases, colonic dysmotility is believed to result from abnormalities of myenteric ganglia and/or associated interstitial cells of Cajal (ICC). To better understand this, we used a recently described HSCR mouse model called *TashT*.

***Methods*:** Intestinal motility parameters were assessed and correlated with extent of aganglionosis as well as with neuronal density in ganglionated regions. The neural composition of the myenteric plexus as well as the status of ICC networks was also evaluated using immunofluorescence.

***Key Results*:** *TashT*$^{Tg/Tg}$ mice display a strong male bias in the severity of both colonic aganglionosis and hypoganglionosis, which are associated with male-specific reduced colonic motility. *TashT*$^{Tg/Tg}$ male mice also exhibit a specific increase of nNos^{+} neurons that is restricted to the most distal ganglionated regions. In contrast, Calretinin^{+} myenteric neurons, Sox10^{+} myenteric glial cells as well as cKit^{+} ICC are not affected in *TashT*$^{Tg/Tg}$ mice.

***Conclusions and Inferences*:** Male-specific impairment of colonic motility in *TashT*$^{Tg/Tg}$ mice is associated with both severe hypoganglionosis and myenteric neuronal imbalance. Considering these parameters in the clinic might be important for the management of post-operative HSCR patients.

Keywords: Chronic constipation, Enteric Nervous System, Hirschsprung disease, Myenteric plexus.

INTRODUCTION

The neural crest-derived enteric nervous system (ENS) is the intrinsic neural network of the entire gastro-intestinal (GI) tract.[1, 2] Buried within the gut wall, the ENS is mainly organized into two major interconnected plexuses: the myenteric (Auerbach's) plexus and the submucosal (Meissner's) plexus. Each plexus consists of interconnected ganglia containing neurons and associated glia. While the myenteric plexus notably controls intestinal motility in collaboration with the interstitial cells of Cajal (ICC) – the pacemaker cells of the bowel, the submucosal plexus regulates several mucosal functions.[3] To perform these tasks, each plexus must contain appropriate density of ganglia as well as adequate proportions of neuron subtypes and glial cells within each ganglion.[4]

Failure of neural crest-derived ENS progenitors to properly reach the distal bowel during prenatal development may cause Hirschsprung disease (HSCR), which affects one in 5000 live births with a 4:1 male to female ratio.[5-7] HSCR is a life-threatening condition characterized by functional obstruction in the distal bowel due to the lack of enteric neural ganglia (aganglionosis). Current treatment consists of surgical resection of the aganglionic segment and anastomosis of upstream ganglionated segment with the anus. However, an important subset of postoperative HSCR patients continue to suffer from long-term altered colonic motility such as fecal incontinence and chronic constipation.[8] Moreover, impaired motility without absence of enteric ganglia is also observed in patients suffering from other enteric neuropathies such as intestinal neuronal dysplasia, intestinal ganglioneuromatosis and isolated hypoganglionosis, to name a few.[9] In all these cases, impaired motility is believed to be due to structural/functional defects of ENS and/or ICC networks.[10-12] However, there is lack of consensus in this regard that clearly calls for further studies.

Animals from HSCR mouse lines with mild phenotypic presentation (e.g. hypoganglionosis and/or ultra-short segment aganglionosis) that do not trigger functional intestinal obstruction have proven especially useful for evaluating the contribution of relatively modest ENS defects to deficits in bowel motility.[13-17] Although gender differences in the penetrance and/or severity of the above phenotypes have been suspected, information regarding the relationship between a given ENS defect (structural abnormalities or neural imbalance) and GI dysmotility in a sex-specific manner is very scarce.[17]

We recently reported the generation of an insertional mutant mouse line called *TashT* in which around 13% of homozygotes (*TashT*$^{Tg/Tg}$) succumb to aganglionic megacolon around weaning age, with a striking 15:1 male to female ratio.[18] Located in a chromosome 10 gene desert, the *TashT* mutation perturbs the activity of silencer elements that are normally involved in the direct repression of the uncharacterized gene *Fam162b* – and potentially other genes – in neural crest-derived ENS progenitors. By a currently unknown mechanism, the *TashT* mutation notably results in the deregulation of key signaling pathways for ENS development (Gdnf/Ret and Edn3/Ednrb) and, consequently, to slower migration of neural crest-derived ENS progenitors in embryonic intestines. What exactly explains the sex bias in megacolon expressivity at the molecular level is also currently unknown. However, at the histological level, we found that it can be explained by the fact that the colon of males is ganglionated, on average, around a threshold level of minimal colonic innervation for FVB/N animals (~80% of total colon length) while the colon of females is ganglionated, on average, just beyond this point.

In this study, we now report that adult *TashT*$^{Tg/Tg}$ mice that do not develop aganglionic megacolon suffer from chronic constipation in a male-specific manner. Extensive characterization of GI motility and myenteric plexus structure/composition suggests that this is due to aganglionosis and/or

hypoganglionosis combined with male-specific neuronal subtypes imbalance in the ganglionated distal colon.

MATERIALS AND METHODS

Animals

All animal studies were conducted in accordance with the guidelines of the Canadian Council on Animal Care (CCAC) and approved by the relevant institutional committee (*Comité institutionnel de protection des animaux*; CIPA reference #650) of University of Quebec at Montreal (UQAM). Both mutant (*TashT*$^{Tg/Tg}$)[18] and wild-type animals are of the same genetic background (FVB/N). All studies were performed using virgin mice between 2-3 months of age, with the exception that body weight was also determined for postnatal day (P) 21 and 28 mice.

Body weight was assessed in the morning using a high precision digital scale (Kilotech KHA5001). For tissue preparation, mice were euthanized following isoflurane anesthesia and relevant bowel segments (duodenum and colon) were immediately dissected out, cut longitudinally along the mesentery, and pinned serosal side down on agar-coated dishes in phosphate buffer saline (PBS). The tissues were fixed overnight at 4ºC in a solution containing 4% phosphate-buffered paraformaldehyde (PFA). After removal of the mucosa/submucosa layers, muscle strips were then dehydrated in methanol and store at -20ºC until labelling. The position of all bowel subregions used in this study is depicted in Supplemental Figure 1.

Staining of acetylcholinesterase activity

The whole colon (from cecum to anus) was collected as above and stained for acetylcholinesterase (AChE) activity essentially as previously described.[19] The length of the myenteric plexus was measured with a millimeter ruler and then converted into percentage of the entire length of the colon. Images were acquired using a DFC-495 camera mounted on a M205FA stereomicroscope (Leica microsystems). To evaluate myenteric plexus density, images were captured at 50X magnification from the proximal, mid, and distal mid colon (MC) as well as from the proximal and mid distal colon (DC) (one representative image per region). For each of these subregions, tissue width was also determined

using a millimeter ruler. For each image, the area occupied by the myenteric plexus was measured in a representative field of view corresponding to a square of fixed dimension (5.4mm^2) using the Image (Adjust - Threshold Color) and Analyze (Measure) functions of Image J. Myenteric plexus density was expressed in percentage of the total area of the field of view. Results for whole MC and DC regions were obtained by averaging the data of the respective subregions.

Immunofluorescence

Dehydrated muscle strips from the duodenum, proximal MC, proximal DC and mid DC were rehydrated and incubated 2 hours at room temperature in blocking solution (10% fetal bovine serum, 0.1% Triton-X100 in PBS). Tissues were incubated with primary antibodies overnight at 4°C and with relevant secondary antibodies for 2 hours at room temperature. Each antibody was diluted in blocking solution (dilution factor and other antibody details can be found in Supplemental Table 1). Muscles strips from the duodenum, proximal MC and mid DC were used for HuC/D / nNos and HuC/D / Calretinin co-labellings. Those from proximal and mid DC as well from distal DC were used for HuC/D / Sox10 and βIII-Tubulin / c-Kit co-labellings, respectively. For each bowel segment, 4µm-thick stacks of 5 fields of view corresponding to a square of fixed dimension (0.3721mm^2) were randomly captured with the 20X objective of a Nikon A1 confocal unit (run with the NIS-Element AR4 software) using standard excitation and emission filters for visualizing DAPI, Alexa Fluor 594 and 647. Neuronal subtypes and glial cell proportions in the myenteric plexus were determined using the Image J cell counter manual function. For each subregion, the sum of Calretinin$^+$, nNos$^+$ and Sox10$^+$ cells from the 5 fields of view were normalized to the total number of HuC/D$^+$ neurons. The total number of HuC/D$^+$ neurons were also used for quantification of neuronal density and expressed in neurons per mm^2.

GI motility assays

Total and proximal (i.e. stomach and small intestine combined) GI transits were assessed using previously described procedures.[20-22] Briefly, mice were administered a solution of 6% carmine red dye (Sigma-Aldrich C1022) dissolved in 0.5% methylcellulose (Sigma-Aldrich 274429) via oral gavage (10µl per gram of weight). For the total GI transit, mice were then returned to individual cages without food, and cages were inspected every 10 min for the presence of red pellets. For each mouse, the total GI transit was expressed as the time (in hour:minutes) required from gavage to expulsion of the first red pellet. For the proximal GI transit, mice were euthanized 15 min after gavage and their small intestine (from duodenum to ileum) was dissected out. The distance travelled by the carmine red dye was measured and expressed in percentage of the length of the entire small intestine. Distal colonic transit was studied via a bead expulsion assay essentially as previously described.[22] Briefly, overnight-fasted mice were anesthetized with 2% isoflurane and a 3mm glass bead was introduced into their colon with a probe over a distance of 2cm from the anus (overlapping both the proximal and mid DC) . The time required for expulsing the glass bead was taken as an estimate of distal colonic transit.

Statistical analysis

Data are presented as the mean (± standard deviation were relevant) with the number (n) of experiments/animals included in figures and/or figure legends. The significance of differences was evaluated using the 2-tailed Student's *t*-test except for Pearson's correlation analyses for which the 1-tailed Student's *t*-test was used. Differences were considered significant for p values ≤ 0.05.

RESULTS

Male-specific impairment of colonic motility in adult *TashT*$^{Tg/Tg}$ mice

We previously reported that almost all *TashT*$^{Tg/Tg}$ animals of weaning age that do not develop megacolon display colonic aganglionosis, with males being more severely affected.[18] No evidence of colon dysmotility was noted for these animals, and they appeared to live as long as wild-type laboratory mice. Yet, GI motility and ENS structure/composition was not analyzed in mature *TashT*$^{Tg/Tg}$ animals. To address this, we began by visually examining their GI tract for possible accumulation of fecal content. These observations revealed a marked propensity to fecal impaction in the colon of adult *TashT*$^{Tg/Tg}$ males when compared to age- and gender-matched wild-type controls (Figure 1A-B and Supplemental Figure 2). Similarly to the male-biased aganglionic megacolon phenotype displayed by this line, *TashT*$^{Tg/Tg}$ females appeared much less affected. Furthermore, we also observed that adult *TashT*$^{Tg/Tg}$ mice gained less weight than age- and gender-matched controls, an outcome again accentuated in males (Table 1).

To further analyze the intestinal motility in *TashT*$^{Tg/Tg}$ mice, transit of carmine red dye and glass bead expulsion assays were used in order to record total and proximal (i.e. stomach and small intestine combined) GI transits as well as distal colonic transit, respectively. Interestingly, a statistically significant increase in the average total GI transit time was specifically observed for *TashT*$^{Tg/Tg}$ males (Figure 2A). Analysis of proximal GI transit and distal colonic transit in isolation further allowed us to find that such reduced GI motility is not global. Indeed, while the proximal GI transit remained unaffected (Figure 2B), the average distal colonic transit time was found to be 9-fold greater in *TashT*$^{Tg/Tg}$ males (Figure 2C). In marked contrast, *TashT*$^{Tg/Tg}$ females were comparable to wild-type controls in all GI motility assays (Figure 2A-C). Taken together, these observations strongly suggest that adult *TashT*$^{Tg/Tg}$ males, but not females, suffer from chronic constipation.

Adult *TashT*$^{Tg/Tg}$ mice exhibit male-biased hypoganglionosis and/or short-segment aganglionosis in the colon

To understand the anatomic basis of the impaired colonic motility described above, we analyzed the gross architecture of the myenteric plexus of adult *TashT*$^{Tg/Tg}$ mice via staining of AChE activity. In accordance with what we previously found with immature *TashT*$^{Tg/Tg}$ animals [18] and as described for a number of other HSCR mouse models [14, 15, 23, 24], this analysis revealed two different yet related ENS structural defects in the colon. For all mature *TashT*$^{Tg/Tg}$ animals, a strong reduction in the density of the myenteric plexus was noted in the mid colon (MC) and the distal colon (DC), and this was found to be combined with distal aganglionosis in approximately half of the studied cases (Figure 3A-C). Such decreased density is not due to colon distention (Supplemental Figure 3) and was also observed in another sample series using anti-HuC/D immunofluorescence (Figure 3D and Supplemental Figure 4). As documented in our prior study [18], the aganglionic segment only contains large extrinsic nerve fibers typically associated with such region. No obvious and/or consistent changes in myenteric plexus density was noted in the proximal colon (PC) and the duodenum (Figure 3A and Supplemental Figure 5). These observations thus indicate that, in comparison to the immature *TashT*$^{Tg/Tg}$ population that includes megacolon-suffering animals [18], the adult population appears enriched in animals having a fully ganglionated colon, although ENS density is significantly reduced in their MC and DC. We believe that the reason why no immature *TashT*$^{Tg/Tg}$ male with a fully ganglionated colon was identified in our previous study is most likely due to the small number of non-megacolon-suffering animals in this group (6 males only).[18] From now on, the subgroup of *TashT*$^{Tg/Tg}$ mice without aganglionosis will be refer to as "hypoganglionic", whereas the subgroup of *TashT*$^{Tg/Tg}$ mice exhibiting both hypoganglionosis and distal aganglionosis will be refer to as "aganglionic".

Sex-stratified analysis of the above phenotypes revealed that, in comparison to females, males are more often subjected to short segment distal aganglionosis. Accordingly, the average extent of aganglionosis

was found to be significantly higher in males compared to females (Figure 3B). Moreover, although the myenteric plexus density for the adult *TashT*$^{Tg/Tg}$ population as a whole appears significantly reduced in comparison to age-matched controls, this decrease is more accentuated in males by a factor of approximately 2-fold (with AChE histochemistry data, 51.6% *versus* 25.8% decrease in the MC and 55.2% *versus* 31.0% decrease in the DC; with HuC/D immunofluorescence data, 41.8% *versus* 18.2% decrease in the MC and 54.5% *versus* 33.1% decrease in the DC) (Figure 3C-D ~~and Supplemental Figure 4B~~). Direct comparison of myenteric plexus density between *TashT*$^{Tg/Tg}$ males and females further revealed statistically significant differences using AChE histochemistry data but not using HuC/D immunofluorescence data (Supplemental Figure 6). Therefore, again in line with the male-biased aganglionic megacolon phenotype previously described for immature *TashT*$^{Tg/Tg}$ mice [18], there is a strong male bias in the expressivity/severity of both hypoganglionosis and short segment aganglionosis in the colon of adult *TashT*$^{Tg/Tg}$ mice.

Correlation between impaired colonic motility and aganglionosis/hypoganglionosis in adult *TashT*$^{Tg/Tg}$ mice

Combining our analyses of myenteric plexus architecture and GI motility pointed towards the existence of a direct link between the identified male-biased myenteric plexus defects (hypoganglionosis and/or short segment aganglionosis) and the male-specific colonic dysmotility. Interestingly, given that almost every tested *TashT* animal was evaluated for all these parameters and that dysmotility was present in both the "hypoganglionic" and "aganglionic" subgroups of *TashT* animals (Figure 2C), this allowed us to assess the relative contribution of different structural defects (i.e. hypoganglionosis without aganglionosis *versus* extent of aganglionosis) to the decreased colon motility. In both cases, modest correlations were detected (Figure 4). The comparison of correlation coefficients revealed a slightly stronger relationship between distal colonic transit time and myenteric plexus density (r = -0.53) than between distal colonic transit time and extent of aganglionosis (r = 0.40). Although statistical

significance was not reached most likely because of the small sample size, these results suggest that both hypoganglionosis and aganglionosis taken separately might partially contribute to the impaired colonic motility observed in *TashT*$^{Tg/Tg}$ males. However, the lack of correlation between distal colonic transit time and myenteric plexus density in *TashT*$^{Tg/Tg}$ females (Figure 4A) combined to the fact that all *TashT*$^{Tg/Tg}$ females (both "hypoganglionic" and "aganglionic") exhibit normal motility (Figure 2C) strongly suggests that these ENS structural defects are not sufficient for explaining the male-specific colon dysmotility of *TashT*$^{Tg/Tg}$ mice.

Male-specific regional alteration of the neurochemical coding of myenteric ganglia in the distal colon of adult *TashT*$^{Tg/Tg}$ mice

As neuronal subtypes and/or glia:neuron ratio imbalance might also contribute to the observed male-specific colonic dysmotility, we subsequently examined the relative abundance of glial cells (Sox10^{+}) as well as the proportion of the main populations of inhibitory (nNos^{+}) and activating (Calretinin^{+}) neurons in myenteric ganglia from the mid DC, using the duodenum as a control region (Figures 5-6). In accordance with the normal motility detected in the anterior GI tract (Figure 2B), the average proportion of Calretinin^{+} and nNos^{+} neurons was similar in the duodenum of wild-type and *TashT*$^{Tg/Tg}$ mice for both genders (Figures 5A', B' and 6A', B'). Similarly, no change was found in the average proportion of Calretinin^{+} neurons as well as in the glia:neuron ratio in myenteric ganglia from the mid DC of *TashT*$^{Tg/Tg}$ animals (Figure 5 and Supplemental Figure 7). However, while the average proportion of nNos^{+} neurons was comparable between wild-type and *TashT*$^{Tg/Tg}$ females either in this same region (Figure 6B-B') or in the distalmost ganglionated region (Supplemental Figure 8), a 110% increase in the average proportion of nNos^{+} neurons was specifically observed in the distal MC of *TashT*$^{Tg/Tg}$ males (Figure 6A-A'). Of note, this 2-fold increase of nitrergic neurons was found to be regionally restricted as no change was observed in the proximal MC (Supplemental Figure 9). Although we do not exclude the possibility that other less abundant neuron subtypes might also be

affected, we believe that such a regionally restricted increase in the main population of relaxing neurons could contribute to the male-specific distal colonic dysmotility.

Status of interstitial cells of Cajal networks in the colon of adult *TashT*$^{Tg/Tg}$ mice

For both human patients and mouse models, altered numbers of interstitial cells of Cajal (ICC) – the GI pacemaker cells – are often observed in association with ENS defects.[25-28] To determine whether these c-Kit^{+} non-neural crest-derived cells might additionally contribute to the male-biased colonic dysmotility of adult *TashT*$^{Tg/Tg}$ mice, their presence and gross distribution were examined at different depth levels within the wall of the hypoganglionic DC. This analysis revealed no overt change in the relative presence and distribution of ICC subpopulations within the longitudinal and circular smooth muscle layers as well as at the level of both the myenteric and deep muscularis plexuses (Supplemental Figure 10). Therefore, these results strongly suggest that the male-biased colonic dysmotility of *TashT*$^{Tg/Tg}$ mice is strictly due to neuronal defects.

DISCUSSION

We previously reported that a subset of *TashT*$^{Tg/Tg}$ mice die from aganglionic megacolon around weaning age, in a strong male-biased manner.[18] Via a comprehensive gender-dependent analysis of multiple ENS characteristics and motility parameters, we now demonstrate that surviving adult *TashT*$^{Tg/Tg}$ mice exhibit diminished colonic motility, again in a male-biased manner. Of note, we also found that such impaired motility can be dissociated from the distal colonic aganglionosis present in an important subset of adult *TashT*$^{Tg/Tg}$ mice. In fact, other data suggest that the cause of the observed male-biased dysmotility could be multifactorial and include a role for male-specific neuronal subtypes imbalance. We believe that these findings could have clinical relevance for the management of postoperative HSCR patients as well as of patients diagnosed for other enteric neuropathies.

Role of myenteric plexus density in the male-biased colonic motility defect of *TashT*$^{Tg/Tg}$ mice

One of the most interesting features of the aganglionosis phenotype of *TashT*$^{Tg/Tg}$ mice is its incomplete penetrance (Figure 3A-B).[18] In this work, we took advantage of this characteristic for specifically assessing the relative contribution of aganglionosis and hypoganglionosis to the male-biased colonic motility defect. Intriguingly, we first observed that not only "aganglionic" but also a high number of what we named "hypoganglionic" *TashT*$^{Tg/Tg}$ animals were present in the group of males exhibiting colonic transit time higher than wild-type controls (Figure 2C). More intriguing was the fact that some of these "hypoganglionic" *TashT*$^{Tg/Tg}$ males were even more severely affected than some "aganglionic" animals. Accordingly, our correlation analyses suggested that distal colonic transit time was more robustly linked to myenteric plexus density rather than to extent of short segment aganglionosis (Figure 4). Although the negative relationship between myenteric plexus density and motility described in our study did not reach statistical significance, this result is in agreement with prior studies reporting altered motility in the hypoganglionic bowel segments of *Ednrb*, *Edn3*, *Gdnf*, *Hand2* and *Raldh* mutant

mice.[14-16, 29, 30] However, it is noteworthy that no such correlation was observed for *TashT*$^{Tg/Tg}$ females. One simple explanation for this sex bias might be that the decrease in myenteric neuronal density of *TashT*$^{Tg/Tg}$ females ranging between 18.2% and 39.4% (Figure 3C-D and Supplemental Figures ~~4B and~~ 8B') is not sufficient for interfering with colonic motility, at least in the FVB/N mouse strain. Indeed, in *TashT*$^{Tg/Tg}$ males, this decrease was calculated to be ≥41.8% (Figure 3C-D ~~and Supplemental Figure 4B~~). Taken together with the data obtained with the other models mentioned above in which neuronal loss was ≥45%,[14, 15, 29, 30] this strongly suggests that a ~40% decrease of myenteric neuronal density might represent a threshold level above which impairment of distal colon motility is more likely to occur.

Role of myenteric neuronal subtypes imbalance in the male-biased colonic motility defect of *TashT*$^{Tg/Tg}$ mice

An alternative and not necessary mutually exclusive possibility for explaining the normal colonic motility of *TashT*$^{Tg/Tg}$ females could be that hypoganglionosis alone is not sufficient for significantly impacting colonic transit. In strong support of this possibility, our analysis of nNos^{+} and Calretinin^{+} neuronal subtypes – the main markers of inhibitory and activating myenteric neurons [31]– revealed a male-specific 2-fold increase of nitrergic neurons restricted to the most distal ganglionated region (Figure 6). Although the proportion of more discrete subtypes might also be affected, we think that doubling the amount of nNos^{+} neurons (from 30% to 63% of all myenteric neurons of the colon) is most likely sufficient by itself to significantly influence motility. Very interestingly, such a regionally restricted increase of nitrergic neurons has also been previously reported in other HSCR mouse models.[15, 17, 32] In this regard, the similarities with mouse models having impaired Edn3/Ednrb signaling are especially striking. Indeed, in both *Ednrb*$^{-/-}$ and *Edn3*$^{-/-}$ mice, an identical ~2-fold increase of nNos^{+} neurons is specifically observed in the most distal ganglionated regions.[15, 32] In *Ednrb*$^{-/-}$ mice,

such increase was also demonstrated to be accompanied by an increase of Vip^+ and a decrease of $ChAT^+$ neurons.[32] On the other hand, it is important to note that a similar robust increase of nitrergic neurons is not found in all HSCR mouse models. Indeed, only slightly increased and even unchanged number of $nNos^+$ myenteric neurons have been reported in *Sox10*$^{Dom/+}$ and *Gdnf*$^{+/-}$ mice, respectively.[15, 17] Therefore, taken together with the fact that Edn3/Ednrb signaling is known to be impaired in *TashT*$^{Tg/Tg}$ enteric neural progenitors[18], these observations suggest a negative role for this signaling pathway in the control of nitrergic neuron numbers that might oppose the apparent positive role of Gdnf/Ret signaling.[33-36] Moreover, the fact that the observed increase in $nNos^+$ neurons is restricted to the most distal ganglionated colon region of *TashT*$^{Tg/Tg}$ males further suggests that it only occurs in response to hypoganglionosis and/or aganglionosis. In agreement with this hypothesis, *nNos* transcript levels are even found to be decreased in *TashT*$^{Tg/Tg}$ e12.5 enteric neural progenitors.[18]

Implications for HSCR and other enteric neuropathies

Despite successful removal of the aganglionic segment and restoration of continuity between the ganglionated colon and the anus, many postoperative HSCR patients continue to suffer from colon motility problems ranging from incontinence to constipation.[8] What exactly explains the variable functional outcomes is currently unknown although this is believed to be due to the nature of the reconnected ganglionated region. Our data are in total agreement with this idea and further suggest that hypoganglionosis above a certain level as well as an increased number of nitrergic neurons both represent important contributing factors. Considering these parameters in the clinic might help predicting the postoperative outcomes and thereby allows for more personalized care of HSCR patients. We are convinced that these parameters might be also useful for the management of patients suffering from other enteric neuropathies.

ACKNOWLEDGEMENTS

The authors thank Denis Flipo (UQAM) for assistance with confocal imaging and all the other members of the Pilon lab for thoughtful discussions about the manuscript.

FUNDING

This work was supported by grants from the Natural Sciences and Engineering Research Council of Canada (NSERC #342093) and from the Canadian Institutes of Health Research (CIHR #MOP-26037) to NP. AMT was supported by a PhD scholarship from the Fonds de la recherche du Québec - Nature et technologies (FRQNT). NP is a Fonds de la Recherche du Québec - Santé (FRQS) Junior2 Research Scholar and the recipient of the UQAM Research Chair on Rare Genetic Diseases. The funders had no role in study design, data collection and analysis, decision to publish, or preparation of the manuscript.

DISCLOSURE

No competing interests declared.

AUTHOR CONTRIBUTION

AMT designed the experiments; AMT and BC performed the experiments, AMT interpreted data; NP supervised the study; AMT and NP wrote the manuscript. All authors reviewed and approved the final manuscript.

REFERENCES

1. Goldstein AM, Hofstra RM and Burns AJ. Building a brain in the gut: development of the enteric nervous system. *Clin Genet*. 2013; 83: 307-16.
2. Lake JI and Heuckeroth RO. Enteric nervous system development: migration, differentiation, and disease. *American journal of physiology Gastrointestinal and liver physiology*. 2013; 305: G1-24.
3. Furness JB. The enteric nervous system and neurogastroenterology. *Nat Rev Gastroenterol Hepatol*. 2012; 9: 286-94.
4. Musser MA and Michelle Southard-Smith E. Balancing on the crest - Evidence for disruption of the enteric ganglia via inappropriate lineage segregation and consequences for gastrointestinal function. *Dev Biol*. 2013; 382: 356-64.
5. Amiel J, Sproat-Emison E, Garcia-Barcelo M, et al. Hirschsprung disease, associated syndromes and genetics: a review. *J Med Genet*. 2008; 45: 1-14.
6. Bergeron KF, Silversides DW and Pilon N. The developmental genetics of Hirschsprung's disease. *Clin Genet*. 2013; 83: 15-22.
7. Obermayr F, Hotta R, Enomoto H and Young HM. Development and developmental disorders of the enteric nervous system. *Nat Rev Gastroenterol Hepatol*. 2013; 10: 43-57.
8. Rintala RJ and Pakarinen MP. Long-term outcomes of Hirschsprung's disease. *Semin Pediatr Surg*. 2012; 21: 336-43.
9. Friedmacher F and Puri P. Classification and diagnostic criteria of variants of Hirschsprung's disease. *Pediatric surgery international*. 2013; 29: 855-72.
10. Bettolli M, De Carli C, Jolin-Dahel K, et al. Colonic dysmotility in postsurgical patients with Hirschsprung's disease. Potential significance of abnormalities in the interstitial cells of Cajal and the enteric nervous system. *J Pediatr Surg*. 2008; 43: 1433-8.
11. Burns AJ, Roberts RR, Bornstein JC and Young HM. Development of the enteric nervous system and its role in intestinal motility during fetal and early postnatal stages. *Semin Pediatr Surg*. 2009; 18: 196-205.
12. Struijs MC, Diamond IR, Pencharz PB, et al. Absence of the interstitial cells of Cajal in a child with chronic pseudoobstruction. *J Pediatr Surg*. 2008; 43: e25-9.
13. Gianino S, Grider JR, Cresswell J, Enomoto H and Heuckeroth RO. GDNF availability determines enteric neuron number by controlling precursor proliferation. *Development*. 2003; 130: 2187-98.
14. Ro S, Hwang SJ, Muto M, Jewett WK and Spencer NJ. Anatomic modifications in the enteric nervous system of piebald mice and physiological consequences to colonic motor activity. *American journal of physiology Gastrointestinal and liver physiology*. 2006; 290: G710-8.
15. Roberts RR, Bornstein JC, Bergner AJ and Young HM. Disturbances of colonic motility in mouse models of Hirschsprung's disease. *American journal of physiology Gastrointestinal and liver physiology*. 2008; 294: G996-G1008.
16. Shen L, Pichel JG, Mayeli T, Sariola H, Lu B and Westphal H. Gdnf haploinsufficiency causes Hirschsprung-like intestinal obstruction and early-onset lethality in mice. *Am J Hum Genet*. 2002; 70: 435-47.
17. Musser MA, Correa H and Southard-Smith EM. Enteric neuron imbalance and proximal dysmotility in ganglionated intestine of the Hirschsprung mouse model. *Cellular and molecular gastroenterology and hepatology*. 2015; 1: 87-101.
18. Bergeron KF, Cardinal T, Toure AM, et al. Male-Biased Aganglionic Megacolon in the TashT Mouse Line Due to Perturbation of Silencer Elements in a Large Gene Desert of Chromosome 10. *PLoS Genet*. 2015; 11: e1005093.
19. Enomoto H, Araki T, Jackman A, et al. GFR alpha1-deficient mice have deficits in the enteric nervous system and kidneys. *Neuron*. 1998; 21: 317-24.
20. Hatzipetros T, Bogdanik LP, Tassinari VR, et al. C57BL/6J congenic Prp-TDP43A315T mice develop progressive neurodegeneration in the myenteric plexus of the colon without exhibiting key features of ALS. *Brain Res*. 2014; 1584: 59-72.

21. Kimball ES, Palmer JM, D'Andrea MR, Hornby PJ and Wade PR. Acute colitis induction by oil of mustard results in later development of an IBS-like accelerated upper GI transit in mice. *Am J Physiol Gastrointest Liver Physiol*. 2005; 288: G1266-73.
22. Li Z, Chalazonitis A, Huang YY, et al. Essential roles of enteric neuronal serotonin in gastrointestinal motility and the development/survival of enteric dopaminergic neurons. *J Neurosci*. 2011; 31: 8998-9009.
23. Wallace AS, Tan MX, Schachner M and Anderson RB. L1cam acts as a modifier gene for members of the endothelin signalling pathway during enteric nervous system development. *Neurogastroenterol Motil*. 2011; 23: e510-22.
24. Soret R, Mennetrey M, Bergeron KF, et al. A collagen VI-dependent pathogenic mechanism for Hirschsprung's disease. *J Clin Invest*. 2015; 125: 4483-96.
25. Ward SM, Ordog T, Bayguinov JR, et al. Development of interstitial cells of Cajal and pacemaking in mice lacking enteric nerves. *Gastroenterology*. 1999; 117: 584-94.
26. Huizinga JD, Berezin I, Sircar K, et al. Development of interstitial cells of Cajal in a full-term infant without an enteric nervous system. *Gastroenterology*. 2001; 120: 561-7.
27. Huizinga JD, Zarate N and Farrugia G. Physiology, injury, and recovery of interstitial cells of Cajal: basic and clinical science. *Gastroenterology*. 2009; 137: 1548-56.
28. Sandgren K, Larsson LT and Ekblad E. Widespread changes in neurotransmitter expression and number of enteric neurons and interstitial cells of Cajal in lethal spotted mice: an explanation for persisting dysmotility after operation for Hirschsprung's disease? *Dig Dis Sci*. 2002; 47: 1049-64.
29. D'Autreaux F, Margolis KG, Roberts J, et al. Expression level of Hand2 affects specification of enteric neurons and gastrointestinal function in mice. *Gastroenterology*. 2011; 141: 576-87, 87 e1-6.
30. Wright-Jin EC, Grider JR, Duester G and Heuckeroth RO. Retinaldehyde dehydrogenase enzymes regulate colon enteric nervous system structure and function. *Dev Biol*. 2013; 381: 28-37.
31. Qu ZD, Thacker M, Castelucci P, Bagyanszki M, Epstein ML and Furness JB. Immunohistochemical analysis of neuron types in the mouse small intestine. *Cell Tissue Res*. 2008; 334: 147-61.
32. Zaitoun I, Erickson CS, Barlow AJ, et al. Altered neuronal density and neurotransmitter expression in the ganglionated region of Ednrb null mice: implications for Hirschsprung's disease. *Neurogastroenterol Motil*. 2013; 25: e233-44.
33. Anderson RB, Stewart AL and Young HM. Phenotypes of neural-crest-derived cells in vagal and sacral pathways. *Cell Tissue Res*. 2006; 323: 11-25.
34. Uesaka T and Enomoto H. Neural precursor death is central to the pathogenesis of intestinal aganglionosis in Ret hypomorphic mice. *J Neurosci*. 2010; 30: 5211-8.
35. Wang H, Hughes I, Planer W, et al. The timing and location of glial cell line-derived neurotrophic factor expression determine enteric nervous system structure and function. *J Neurosci*. 2010; 30: 1523-38.
36. Yan H, Bergner AJ, Enomoto H, Milbrandt J, Newgreen DF and Young HM. Neural cells in the esophagus respond to glial cell line-derived neurotrophic factor and neurturin, and are RET-dependent. *Dev Biol*. 2004; 272: 118-33.

FIGURE LEGENDS

Figure 1. Fecal retention in the colon of adult *TashT*$^{Tg/Tg}$ males. **(A)** Representative images of whole colons from adult wild-type and *TashT*$^{Tg/Tg}$ mice. Numbers are arbitrary units (A.U.) assigned by someone who was blinded to genotype in order to grade fecal impaction: 1- well separated pellets as observed in the colon of wild-type mice (arrowheads); 2 and 3 - small and high numbers of compacted feces, respectively (arrows). Note that *TashT*$^{Tg/Tg}$ males display markedly higher fecal impaction in comparison to *TashT*$^{Tg/Tg}$ females and wild-type controls. **(B)** Quantitative analyses using the arbitrary units described in A (**$p \leq 0.001$; Student's *t*-test).

Figure 2. Impaired gastrointestinal (GI) motility in adult *TashT*$^{Tg/Tg}$ males. **(A)** Total GI transit evaluated by the time (hour:minutes) required for expelling the first red pellet following oral gavage with carmine red dye. Note that the average time of total GI transit is increased in *TashT*$^{Tg/Tg}$ males in comparison to *TashT*$^{Tg/Tg}$ females and wild-type controls. **(B)** Proximal GI transit evaluated by the distance traveled by the carmine red dye 15 min after gavage and expressed in percentage of the total length of the small intestine. **(C)** Distal colonic transit evaluated by bead latency assay and expressed in min. Note that the average time of distal colonic transit in *TashT*$^{Tg/Tg}$ males is 9-fold greater in comparison to *TashT*$^{Tg/Tg}$ females and wild-type controls (*$p \leq 0.05$; **$p \leq 0.001$; Student's *t*-test).

Figure 3. Adult *TashT*$^{Tg/Tg}$ mice exhibit male-biased short-segment aganglionosis and hypoganglionosis. **(A)** Representative images of whole-mount staining of acetylcholinesterase activity in the myenteric plexus of adult wild-type and *TashT*$^{Tg/Tg}$ mice. Note that all *TashT*$^{Tg/Tg}$ animals exhibit hypoganglionosis in the mid colon whereas either hypoganglionosis or aganglionosis is observed in the distal colon. Arrow and arrowheads indicate myenteric ganglia and extrinsic nerve fibers, respectively.

Scale bar, 1mm. **(B)** Quantification of the extent of aganglionosis expressed in percentage of total colon length. The average extent of aganglionosis is significantly increased in *TashT*$^{Tg/Tg}$ males compared to females. **(C)** Quantitative analysis of myenteric plexus density in ganglionated regions using images similar to those shown in (A), taken from the proximal, mid and distal mid colon (MC) and from the proximal and mid distal colon (DC). Note that the aganglionic distal DC was not included for these analyses. The area occupied by the myenteric plexus was measured from representative fields of view and expressed in percentage of the total area of the field of view (5.4mm^2). Each single value corresponds to the average of either three (proximal, mid and distal MC) or two (proximal and mid DC) subregions (using one representative field of view per subregion). (**D**) Quantitative analyses of anti-HuC/D immunofluorescence data in ganglionated regions of *TashT*$^{Tg/Tg}$ colons using images such as those shown in Supplemental Figure 4, taken from the proximal MC and mid DC. For each subregion, the myenteric neuronal density was calculated from 5 fields of view and expressed in number of HuC/D$^+$ cells per mm^2. Note that a significant decrease of myenteric plexus density and neuron numbers is observed in *TashT*$^{Tg/Tg}$ mice of both genders but is more pronounced in males (*$p \leq 0.05$; (**$p \leq 0.001$; ***$p \leq 0.0001$; Student's *t*-test).

Figure 4. Correlation between distal colonic transit time and extent of hypoganglionosis or aganglionosis exhibited by adult *TashT*$^{Tg/Tg}$ mice. (A) Plot of distal colonic transit time (Figure 2C) relative to average myenteric plexus density in the distal colon (combining proximal and mid but excluding distal subregions) of "hypoganglionic" *TashT*$^{Tg/Tg}$ mice (Figure 3C). Distal colonic transit time tends to be inversely correlated to myenteric plexus density, but only for *TashT*$^{Tg/Tg}$ males. **(B)** Plot of distal colonic transit time (Figure 2C) relative to the extent of colonic aganglionosis in "aganglionic" *TashT*$^{Tg/Tg}$ males (Figure 3B). Only a moderate positive correlation that does not reach statistical significance is observed. r, Pearson's correlation coefficient; *p*, Student's *t*-test value.

Figure 5. The proportion of Calretinin^{+} myenteric neurons is unaffected in adult *TashT*$^{Tg/Tg}$ mice. **(A-B)** Representative Z projection micrographs of myenteric ganglia from the mid DC of male (A) and female (B) mice double-labelled with anti-Calretinin (green) and anti-HuC/D (red) antibodies. Scale bar, 50µm. (**A'-B'**) Quantitative analyses of the average proportion of Calretinin^{+} myenteric neurons in the duodenum and mid DC. No statistically significant difference is observed between *TashT*$^{Tg/Tg}$ mice and age- and gender-matched controls. DC, distal colon.

Figure 6. Male-specific and regionally-restricted increase of nNos^{+} neuron numbers in myenteric ganglia of adult *TashT*$^{Tg/Tg}$ mice. (A-B) Representative Z projection micrographs of myenteric ganglia from the mid DC of male (A) and female (B) mice double-labelled with anti-nNos (green) and anti-HuC/D (red) antibodies. Scale bar, 50µm. (**A'-B'**) Quantitative analyses of the average proportion of nNos^{+} myenteric neurons in the duodenum and mid DC. The average proportion of nNos^{+} myenteric neurons is specifically increased in the mid DC of *TashT*$^{Tg/Tg}$ males (*$p \leq 0.05$; Student's *t*-test). DC, distal colon.

Supplemental Figure 1. Illustration of a mouse gastrointestinal tract showing the position of the subregions that were used in this study.

Supplemental Figure 2. Complete visual analysis of fecal impaction in *TashT*$^{Tg/Tg}$ mice All colons from adult *TashT*$^{Tg/Tg}$ mice used to quantify fecal impaction in Figure 1B are shown along with representative images of control colons.

Supplemental Figure 3. Colonic distention cannot explain the robust decrease in myenteric plexus density displayed by adult *TashT*$^{Tg/Tg}$ males. Plot of MC width (combining proximal, mid and distal subregions) relative to corresponding myenteric plexus density of adult wild-type and *TashT*$^{Tg/Tg}$ male mice (n=7 animals for each). Each single value corresponds to an individual subregion. No correlation is observed between the colon width and the myenteric plexus density for both wild-type and *TashT*$^{Tg/Tg}$ mice (r, Pearson's coefficient; p: Student's *t*-test value). MC, mid colon.

Supplemental Figure 4. Male-biased reduced myenteric neuronal density in the colon of adult *TashT*$^{Tg/Tg}$ mice. ~~(A)~~ Representative Z projection micrographs of myenteric neurons from the proximal MC and mid DC of adult wild-type and *TashT*$^{Tg/Tg}$ males labelled with an anti-HuC/D (grey) antibody. Scale bar, 100µm. ~~**(B)** Quantitative analyses of myenteric neuron numbers in proximal MC and mid DC. The average number of myenteric neurons is reduced in all *TashT*$^{Tg/Tg}$ mice, an outcome that appears more pronounced in males (**$p \leq 0.001$; ***$p \leq 0.0001$; Student's *t*-test). MC, mid colon. DC, distal colon.~~

Supplemental Figure 5. The myenteric neuronal density is unaffected in the duodenum of adult *TashT*$^{Tg/Tg}$ mice. (**A-B**) Representative Z projection micrographs of myenteric neurons from the duodenum of adult wild-type and *TashT*$^{Tg/Tg}$ males (A) or females (B) labelled with an anti-HuC/D (grey) antibody. Scale bar, 100µm. (**A'-B'**) Quantitative analyses of myenteric neuron numbers in the duodenum. The average neuronal density is comparable between *TashT*$^{Tg/Tg}$ and age- and gender-matched wild-type mice.

Supplemental Figure 6. Inter-gender comparative analyses of myenteric plexus density and neuron numbers in age-matched *TashT*$^{Tg/Tg}$ mice. (**A**) The average myenteric plexus density as determined using AChE histochemistry is significantly reduced in *TashT*$^{Tg/Tg}$ males compared to females. As described in Figure 3C, each single value in MC and DC corresponds to the average of three or two subregions, respectively. (**B**) The average number of HuC/D^{+} neurons per mm^2 is smaller in *TashT*$^{Tg/Tg}$ males relative to females (*$p \leq 0.05$; **$p \leq 0.001$; ***$p \leq 0.0001$; Student's *t*-test). MC, mid colon. DC, distal colon.

Supplemental Figure 7. The neuron:glia ratio within myenteric ganglia is unchanged in the distal colon of adult *TashT*$^{Tg/Tg}$ mice. (A) Representative Z projection micrographs of myenteric ganglia from the proximal and mid DC of adult wild-type and *TashT*$^{Tg/Tg}$ mice double-labelled with anti-Sox10 (green) and anti-HuC/D (red) antibodies. Scale bar, 100µm. **(B)** Quantitative analyses of the neuron:glia ratio in wild-type and *TashT*$^{Tg/Tg}$ mice of both genders. No statistically significant difference is observed between *TashT*$^{Tg/Tg}$ mice and age- and gender-matched controls. DC, distal colon.

Supplemental Figure 8. The proportion of nNos^{+} myenteric neurons is unaffected in the hypoganglionic DC of adult *TashT*$^{Tg/Tg}$ females. (**A-B**) Representative Z projection micrographs of myenteric ganglia from the distal DC of age-matched wild-type and *TashT*$^{Tg/Tg}$ female mice labelled with anti-HuC/D (red) and anti-nNos (green) antibodies (A) or with anti-HuC/D (grey) only (B). Scale bars, 50µm (A) and 100µm (B). (**A'-B'**) Quantitative analyses of the average proportion of nNos^{+} myenteric neurons and the average neuronal density in the distal DC. The average proportion of nNos^{+}

myenteric neurons is comparable between wild-type and *TashT*$^{Tg/Tg}$ females (A') despite a significant decrease in the average neuronal density (B') (*$p \leq 0.05$; Student's *t*-test). DC, distal colon.

Supplemental Figure 9. The proportion of nNos^{+} myenteric neurons is not altered in the proximal MC of adult *TashT*$^{Tg/Tg}$ males. (**A**) Representative Z projection micrographs of myenteric ganglia from the proximal MC of age-matched wild-type and *TashT*$^{Tg/Tg}$ male mice double-labelled with anti-nNos (green) and anti-HuC/D (red) antibodies. Scale bar, 50µm. (**B**) Quantitative analyses of the average proportion of nNos^{+} myenteric neurons in the proximal MC. No difference is observed between wild-type and *TashT*$^{Tg/Tg}$ mice. MC, mid colon.

Supplemental Figure 10. Distribution of interstitial cells of Cajal (ICC) in hypoganglionic distal DC of adult *TashT*$^{Tg/Tg}$ mice. Representative Z projection micrographs of ICC as well as myenteric and deep muscularis neuronal plexuses from the distal DC of adult wild-type and *TashT*$^{Tg/Tg}$ mice labeled with anti-c-Kit (green) and anti-βIII-Tubulin (red), respectively. ICC-LM and ICC-CM are ICC located within the longitudinal and circular smooth muscle layers, respectively. ICC-MY and ICC-DMP are ICC present at the level of the myenteric and the deep muscularis plexuses, respectively. No overt change is detected in the distribution of these different ICC subpopulations between adult wild-type and *TashT*$^{Tg/Tg}$ mice. Scale bar, 100µm.

Table 1. Comparison of body weight between wild-type and *TashT*$^{Tg/Tg}$ mice at P21, P28 and 2-3 months.

Gender	Genotype	Age		
		P21	P28	2-3 months
♂	Wild-type	12 ± 1 (*n=25*)	19 ± 1 (*n=25*)	28 ± 1 (*n=11*)
	TashT$^{Tg/Tg}$	10 ± 1 (*n=14*)	16 ± 1 (*n=15*)	22 ± 1 (*n=10*)
	% difference	-16.67%	-15.78%	-21.43%
	p-value	5,279 E-06	1,008 E-05	1,823 E-09
♀	Wild-type	12 ± 1 (*n=11*)	17± 1 (*n=11*)	22 ± 2 (*n=12*)
	TashT$^{Tg/Tg}$	11 ± 1 (*n=25*)	15 ± 1 (*n=25*)	20 ± 1 (*n=13*)
	% difference	-8.33%	-11.76%	-9.09%
	p-value	0,018	3,244 E-05	0,012

Supplemental Table 1. List of primary and secondary antibodies used in this study.

Antibody	Dilution	Host species	RRID number	Source
Anti-HuC/D	1 :500	Mouse	AB_2314656	Molecular Probes, A-21271
Anti-Calretinin	1 :500	Goat	AB_10000342	Swant, CG1
Anti-nNos	1 :500	Rabbit	AB_91824	Millipore, AB5380
Anti-Sox10	1 :500	Goat	AB_2195374	Santa Cruz Biotechnology, sc-17342
Anti-C-kit	1 :500	Goat	AB_354750	Cederlane (Canada), AF1356
Anti-βIII-Tubulin	1 :200	Mouse	AB_2256751	Abcam, ab78078
Anti-Mouse Alexa Fluor 647	1 :500	Donkey	AB_2340862	Jackson Immuno Research, 715-605-150
Anti-Rabbit Alexa Fluor 594	1 :500	Donkey	AB_2340621	Jackson Immuno Research, 711-585-152
Anti-Goat Alexa Flour 594	1 :500	Bovine	AB_2340884	Jackson Immuno Research, 805585180

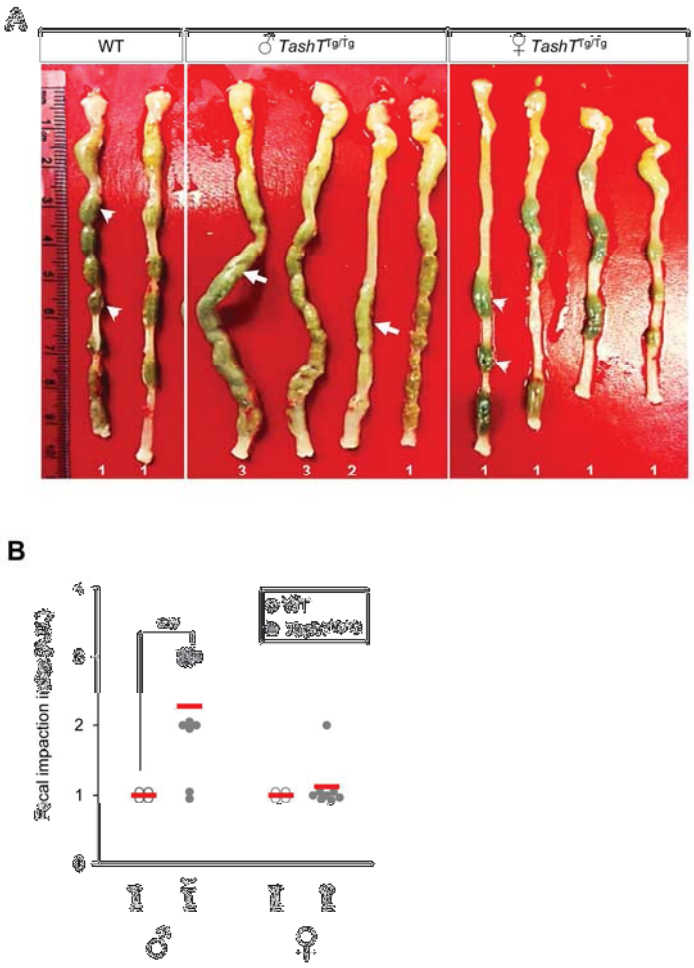

Fig.1
194x254mm (300 x 300 DPI)

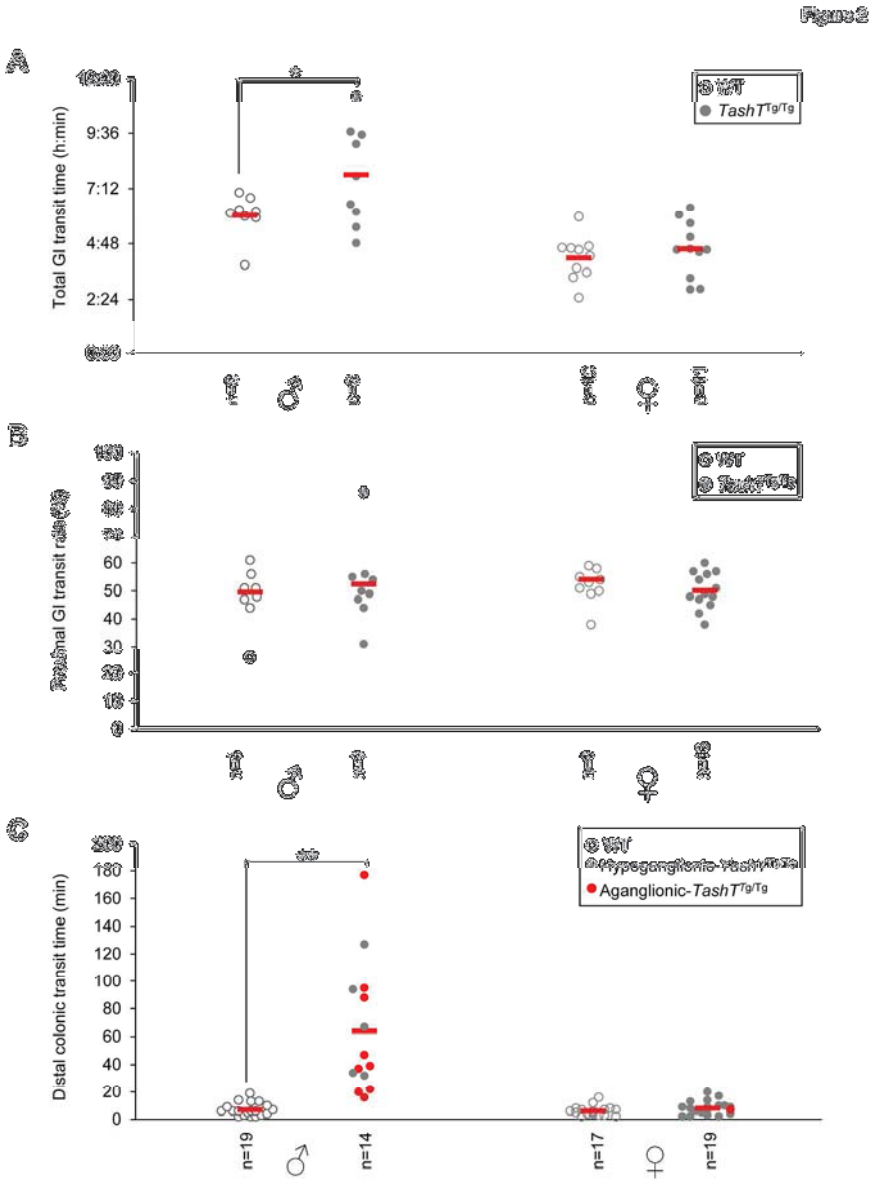

Fig.2
194x254mm (300 x 300 DPI)

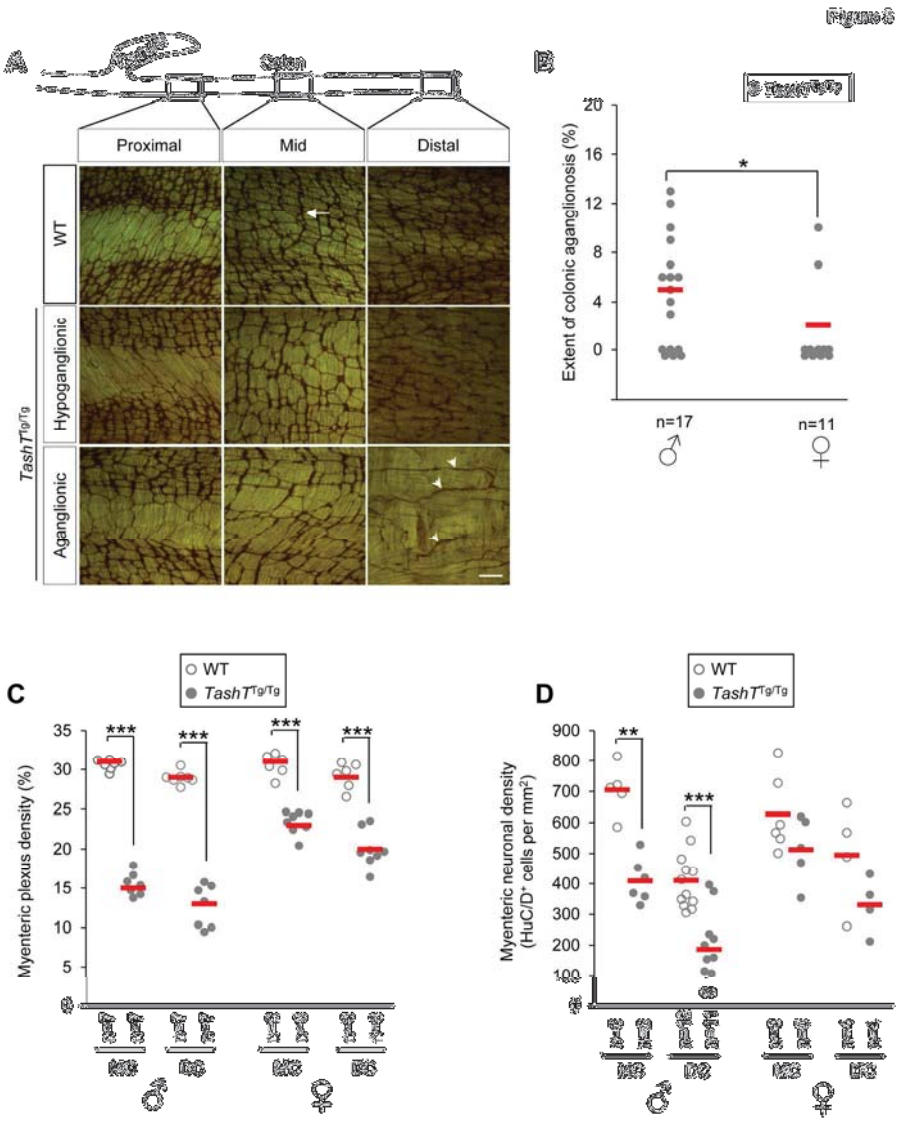

Fig.3
199x254mm (300 x 300 DPI)

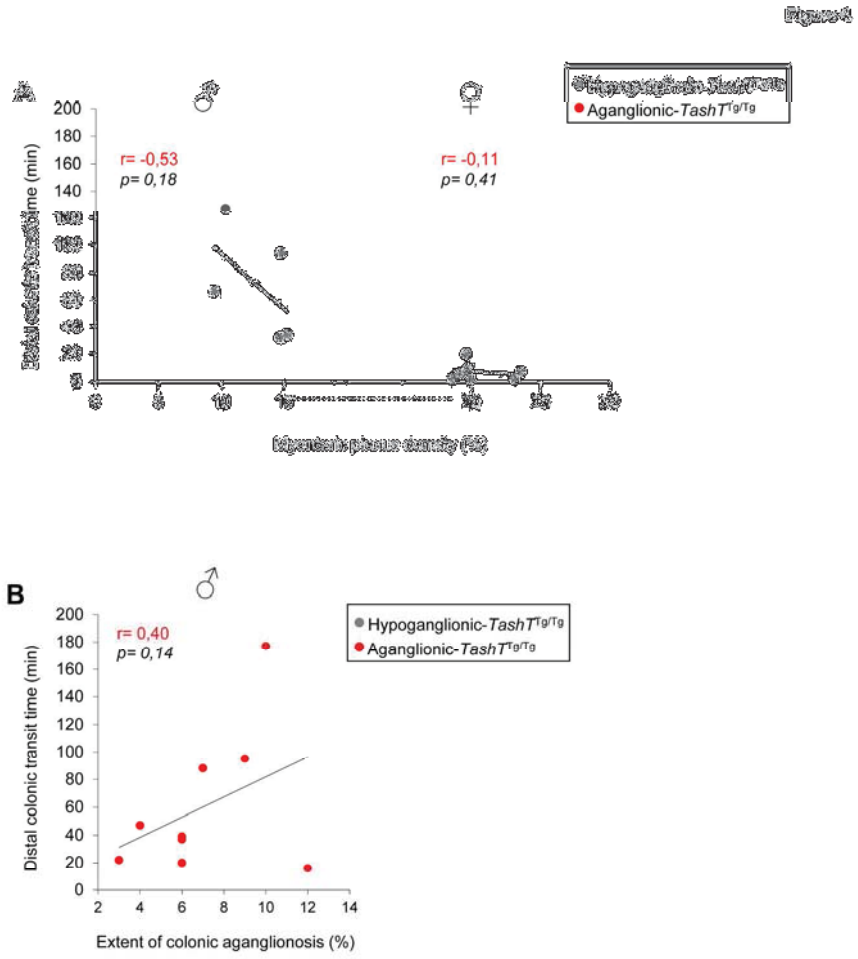

Fig.4
194x254mm (300 x 300 DPI)

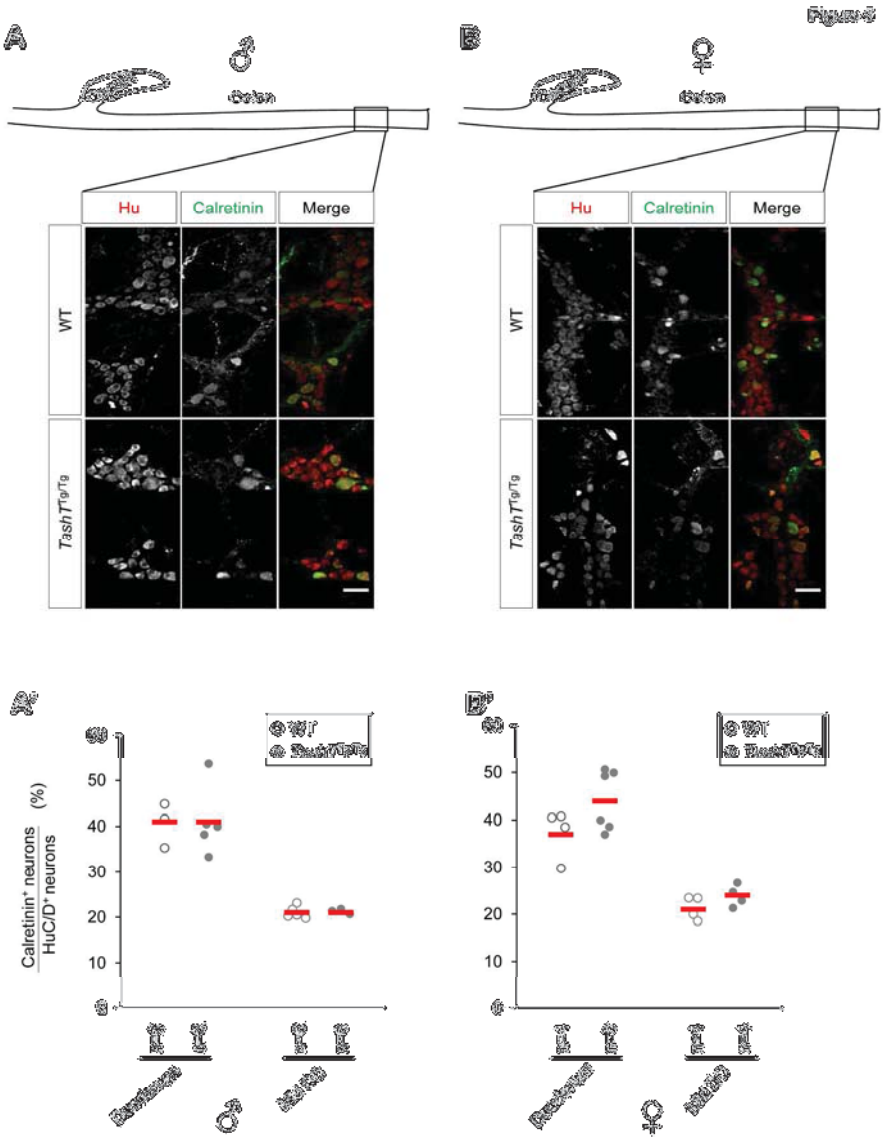

Fig.5
195x253mm (300 x 300 DPI)

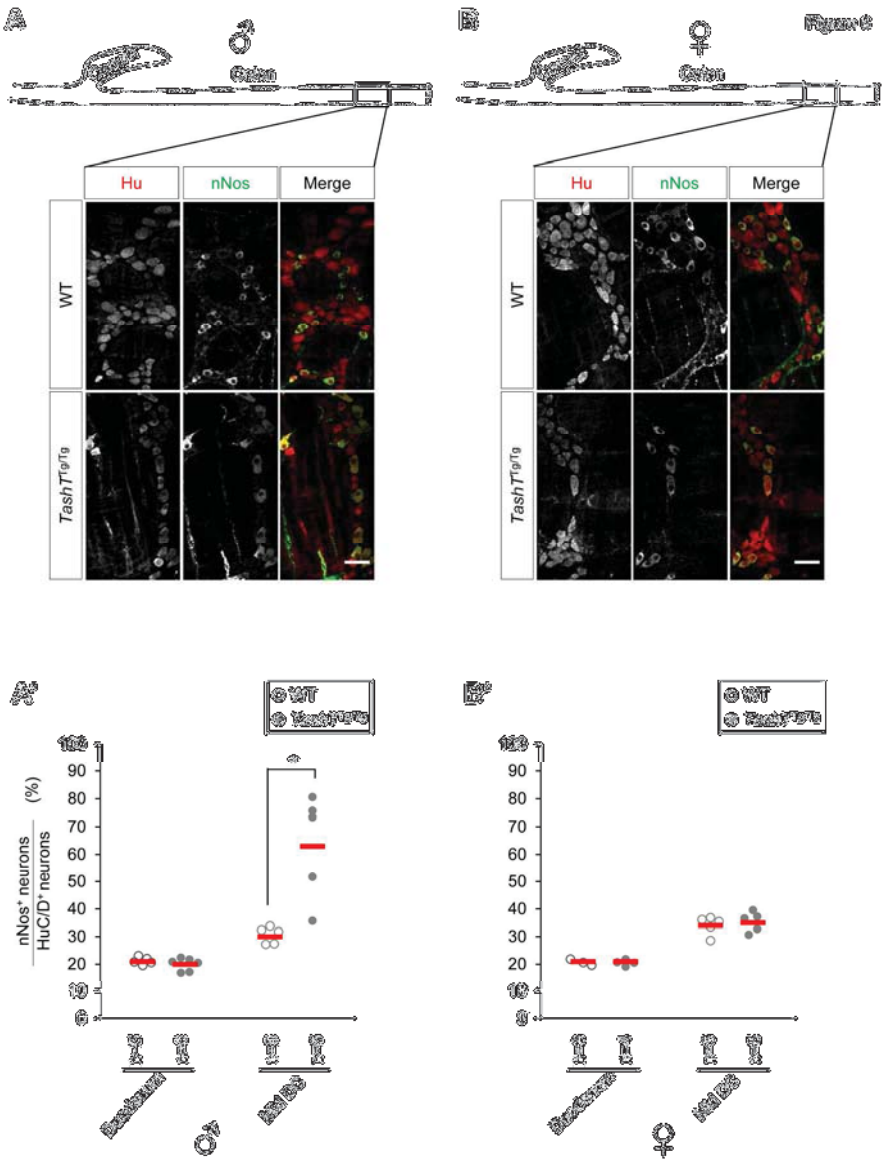

Fig.6
197x254mm (300 x 300 DPI)

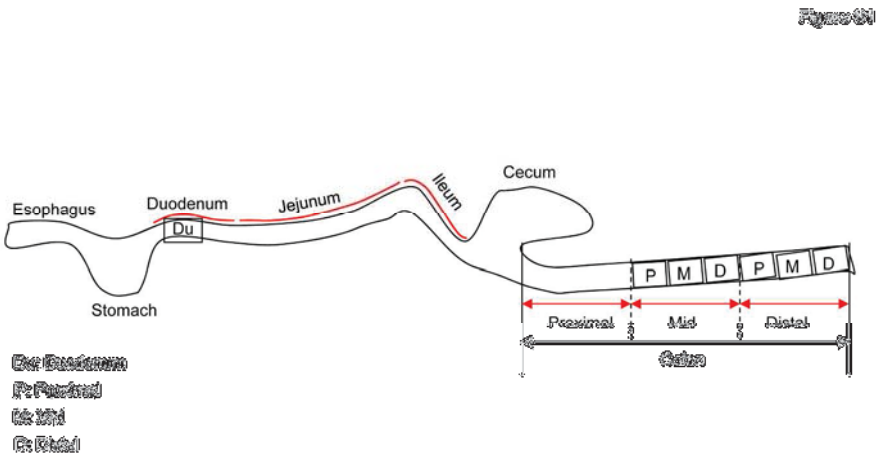

Fig.S1
194x254mm (300 x 300 DPI)

Fig.S2
194x254mm (300 x 300 DPI)

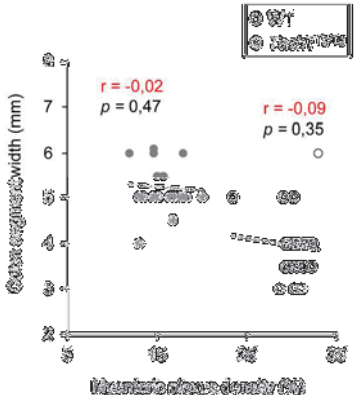

Fig.S3
194x254mm (300 x 300 DPI)

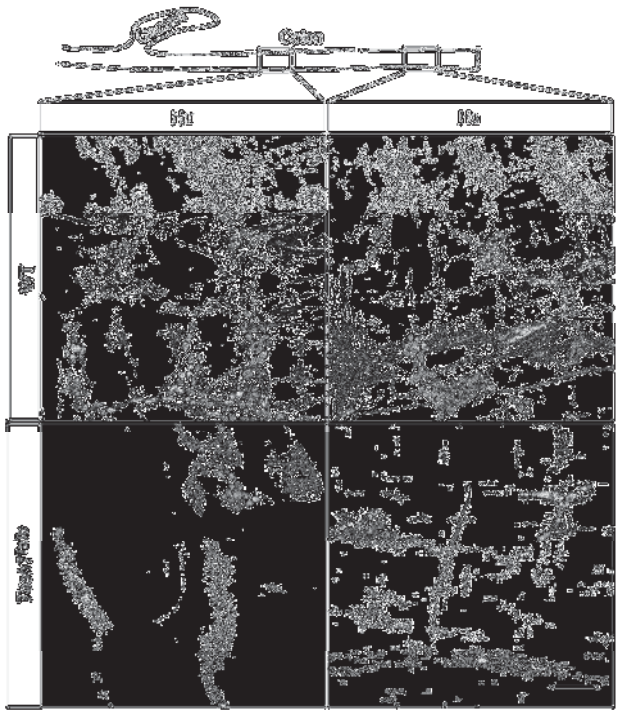

Fig.S4
193x254mm (300 x 300 DPI)

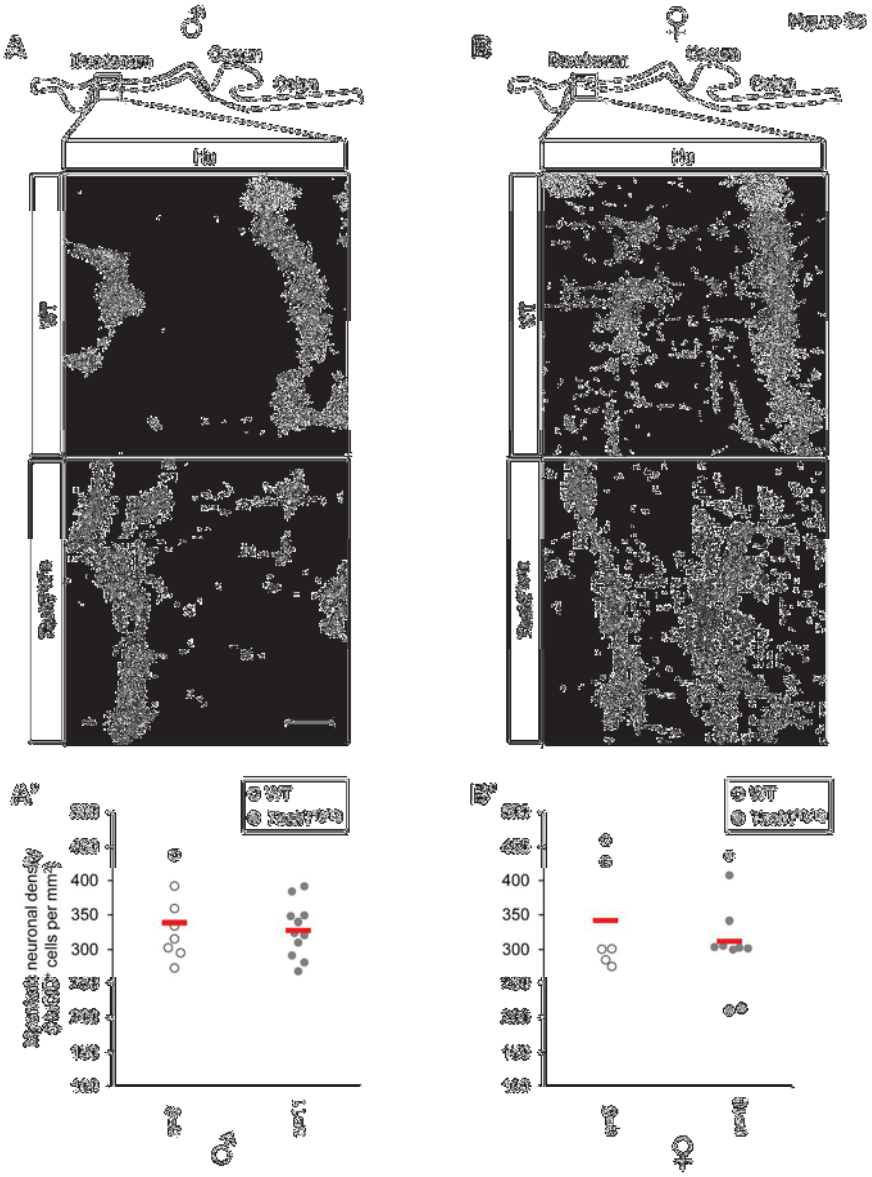

Fig.S5
195x255mm (300 x 300 DPI)

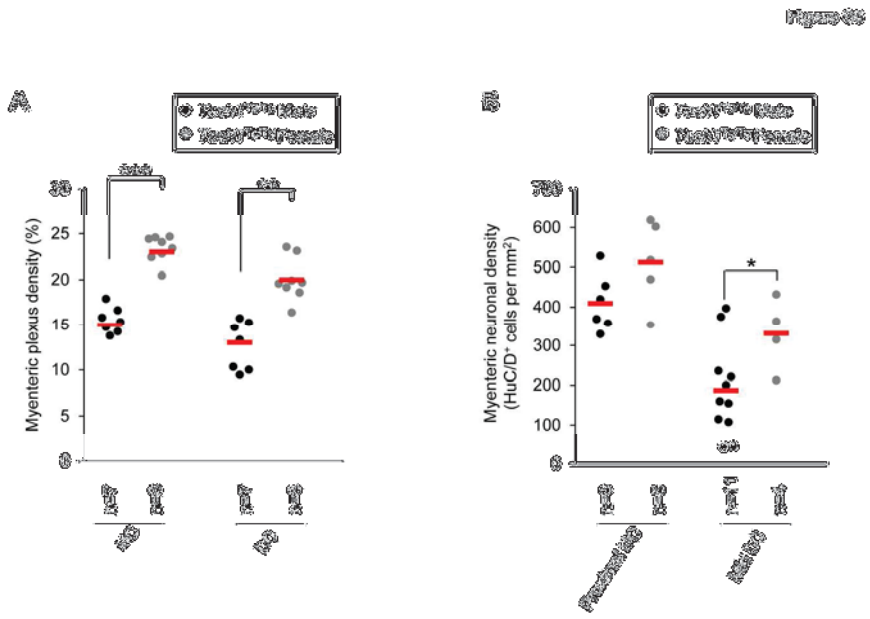

Fig.S6
193x254mm (300 x 300 DPI)

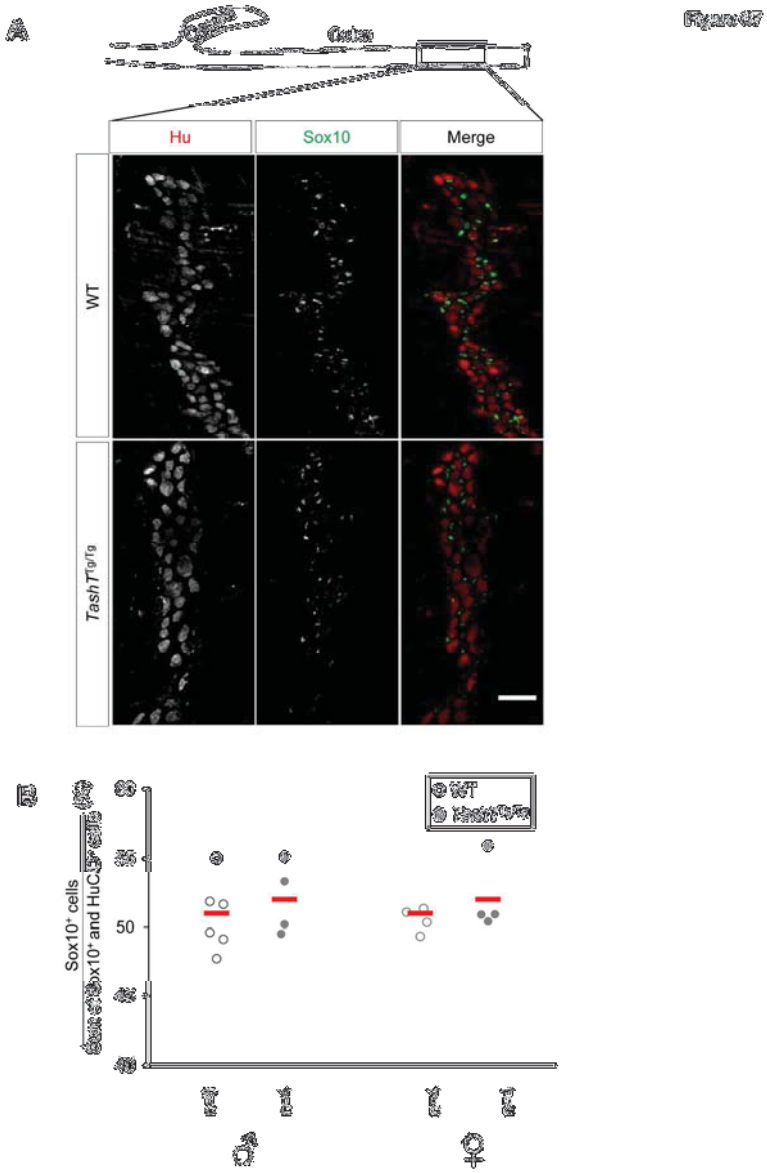

Fig.S7
194x254mm (300 x 300 DPI)

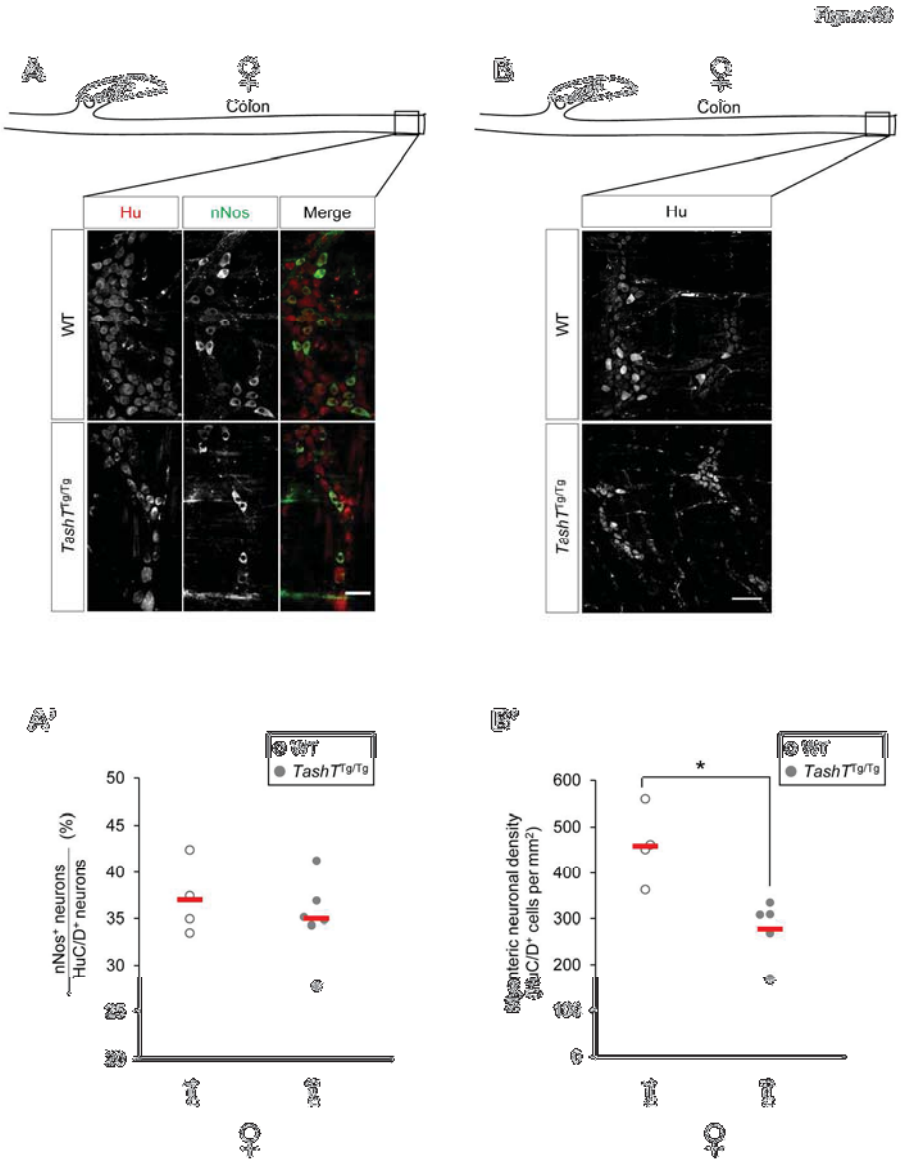

Fig.S8
195x253mm (300 x 300 DPI)

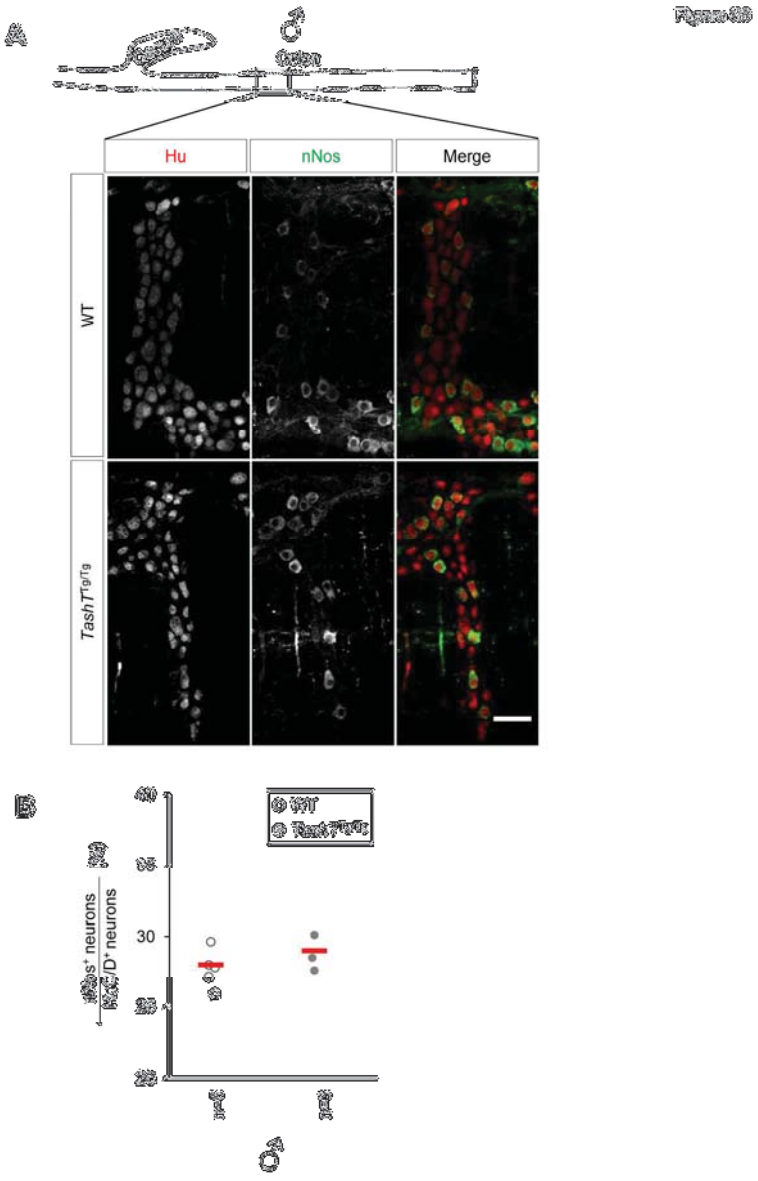

Fig.S9
194x254mm (300 x 300 DPI)

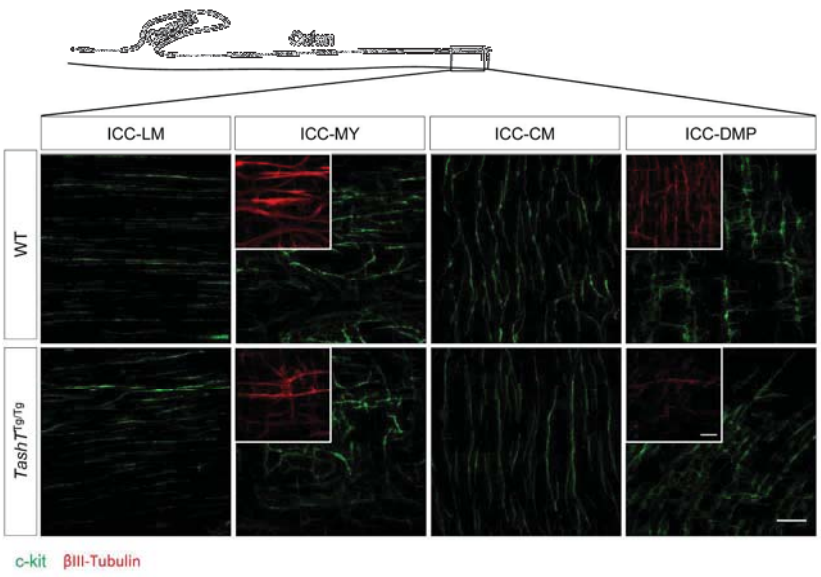

Fig.S10
190x254mm (300 x 300 DPI)